NUMERICAL SIMULATION OF CO_2 ABSORPTION BY AMP SOLUTION IN STRUCTURED PACKING WITH DIFFERENT PARAMETER CONDITION

Xu Zuo[a], and Hongtao KAO[a]*

[a] College of Materials Science and Engineering, Nanjing Tech University, Nanjing 211816, China

*Corresponding author, E-mail: kaoht@163.com

The FLUENT software is utilized in this research to simulate the carbon dioxide absorption process by 2-amino-2-methyl-1-propyl alcohol through numerical simulation. A mathematical model is established to represent the mass transfer process between the 2-amino-2-methyl-1-propyl alcohol solution and carbon dioxide. Various operating parameters, such as the molar fraction of the solution, gas mass fraction, pressure, and gas flow velocity, are investigated to calculate the absorption efficiency of carbon dioxide under different conditions. The distribution of the product reveals that the 2-amino-2-methyl-1-propyl alcohol carbamate product more readily infiltrates the surface of the unit model when the gas phase velocity is relatively low. In contrast, the product 2-amino-2-methyl-1-propyl alcohol carbamate tends to accumulate in the upper half of the unit model when the gas phase velocity is relatively high. Sixteen simulation conditions are summarized to determine the optimal parameters. These optimal parameters include a 2-amino-2-methyl-1-propyl alcohol molar fraction of 0.4, atmospheric pressure, a flue gas flow velocity of 0.0737 m/s, and a carbon dioxide mass fraction of 0.12. This research serves as a valuable reference for engineering applications related to carbon dioxide absorption using 2-amino-2-methyl-1-propyl alcohol solutions, providing essential technical support in the fight against climate change.

Key words: *AMP; numerical simulation; CO_2 absorption; carbon emission reduction; chemisorption*

1. Introduction

In recent years, with the aggravation of the greenhouse effect, global temperatures have continued to rise, and the emission of greenhouse gas carbon dioxide (CO_2) has garnered increasing concern. Industrial production relies on coal, petroleum, natural gas, and other sources as energy [1], making them the primary sources of CO_2 emissions in industrial processes following combustion and usage. Globally, coal is the main fuel for power generation, with its share reaching 36.4% in 2019 [2]. For the cement industry, CO_2 emissions account for about 7-8% of total global CO_2 emissions [3]. It is therefore important to limit and sanction anthropogenic greenhouse gas and related sectoral CO2 emissions [4].

Given the current development landscape, the thermal power and cement industries employ three main methods to reduce carbon emissions: substituting traditional fuels with low-carbon alternatives, enhancing unit heat efficiency, and implementing Carbon Capture and Storage (CCS) technology [5]. In practical production, the availability of fuel sources for cement plants in each area, theoretical heat consumption limits for mineral products, and cement kiln clinker without viable alternatives, as well as potential disruptions to the cement production process by these methods, can impact the quality of the produced cement. Consequently, there is a growing interest in CCS technology that can be applied in the thermal power and cement industries.

Within the realm of CCS technology, post-combustion carbon capture technology and oxygen-enriched combustion technology are considered to be particularly well-suited for industrial applications. Oxygen-enriched combustion produces exhaust with a high carbon dioxide concentration, which is advantageous for the subsequent carbon dioxide capture process after water condensation [6]. Post-combustion carbon capture technology involves the enrichment and purification of CO_2 in post-combustion flue gas using absorbents and the reutilization of purified CO_2 in industrial production after compression and liquefaction [7]. CO_2 absorption entails the flow of gas and chemical absorbents in a vertical tower (such as a packed tower) in a countercurrent mode, ensuring thorough mixing of gas and liquid through tower structures to maximize contact and ensure efficient gas absorption [8]. Presently, organic amine solutions are the most widely used in the industry.

Ethanolamine (MEA) was among the first amines used as an absorbent in the industry. However, in practical applications, several drawbacks were identified. MEA as an absorbent requires relatively high temperatures, increasing energy consumption and leading to more severe equipment corrosion [9]. As a result, current research is focused on reducing the energy consumption during MEA regeneration in the desorption process [10].

Benamor and Aroua [11] used a laboratory stirred reactor and analyzed the experimental data for the determination of CO_2 uptake at different concentrations of methyl diethanolamine (DETA) at different temperatures and calculated the kinetic parameters related to the reaction , such as the number of reaction stages and the reaction rate constant. Feng *et al.* [12] and Kierzkowska-Pawlak *et al.* [13] found that in terms of uptake rate, CO_2 uptake by N-Methyldiethanolamine (MDEA) was slower. Consequently , Ahmady [14] and colleagues proposed mixed CO_2 absorption using an ionic liquid, [bmim][BF_4], in combination with MDEA. Their research on the absorption kinetics of CO_2 in MDEA+[bmim][BF_4] water solutions at different temperatures and ionic solution concentrations, using a stirring tank reactor, confirmed that the amount of CO_2 absorbed in the solution steadily increased as the ionic liquid concentration rose. Also, Glazyrin *et al.* [15] have shown that by reacting wastewater with flue gas components, solutions with regenerative properties are generated and used for the regeneration of ion exchangers for water treatment and flue gas purification.

The MEA and DETA mentioned above are commonly used alkanolamines in the industry. They have the capability to form stable carbamic acid esters, which possess the activity to facilitate rapid

chemical reactions. However, it's important to note that the formation of stable carbamic acid esters can result in significantly high regeneration costs [16]. Except for currently widely used amine solution absorbents, sterically hindered amines have been gaining attention due to their relatively higher efficiency in CO_2 absorption. Furthermore, the steric hindrance effect significantly impacts the stability of the generated carbamic acid ester, resulting in low stability and easy hydrolysis into bicarbonate ions [17]. Sterically hindered amines also possess favorable thermodynamic properties, resistance to degradation, and high absorptivity, among other advantages [18].

Sartori and Savage [19] were among the first to propose two types of sterically hindered amines: (1) first amine is classified as a secondary amine wherein the amino group is attached to at least one secondary or tertiary carbon; and (2) primary amines with an amino group connected to a tertiary carbon. Various sterically hindered amines have been identified, including 2-piperidinol (2-PE), 2-piperinol (2-PM), 2-amino-2-ethyl-1,3-propanediol (AEPD), 2-amino-2-hydroxymethyl-1,3-propanediol (AHPD), and 2-amino-2-methyl-1-propyl alcohol (AMP). According to Khan *et al*. [20], the regeneration performance of AMP was experimented with for two amine loaded solvents in a temperature range and vacuum, and it was found that the CO_2 loading capacity of AMP was higher than the MEA value, and AMP had a better regeneration efficiency of 97.85% than MEA. At a regeneration temperature of 382 K, the regeneration efficiency was 85.4%. The energy intensity of AMP regeneration was found to be 41.7% lower than MEA in terms of reboiler heat load. Challenges in actual operation, such as high temperatures, high pressure, toxic substances, and complex equipment, have led to difficulties in conducting relevant experiments in factories.

With advancements in computer technology, carbon capture using computational fluid dynamics (CFD) has emerged as a novel research method [21]. Compared to experimental methods, CFD simulations require less time, can be easily repeated for verification and to test varying conditions, and offer greater flexibility in changing parameters. The combination of CFD technology and practical production provides valuable insights for the application of CO_2 absorption in industrial settings. This paper primarily focuses on researching the influencing factors and absorption rules for CO_2 absorption using AMP as an absorbent.

Three-dimensional modeling utilizes the unit filler in the Mellapak 250Y-type filler, and CFD technology simulates the process of AMP solution and CO_2 within the unit filler. Calculations are conducted to explore CO_2 absorption by AMP in the unit model, considering different AMP molar fractions, CO_2 mass fractions, various pressures, and gas-liquid flow velocities. A multifactor analysis is employed to determine the optimal ratios of each factor, facilitating a better understanding of fluid distribution and mixing in the absorption process. This study utilizes AMP solutions for efficient absorption of CO_2 to mitigate climate change and greenhouse gas emissions. Through simulations using Fluent software, we were able to accurately analyze the kinetics of CO_2 absorption in solution, mass transfer characteristics, and the effects of various parameters in the solution, which opens up new possibilities for low-energy carbon capture technologies. Secondly, this technology is practically feasible for CO_2 capture in industrial emissions, which is expected to help companies achieve their

emission reduction targets and meet the urgent global need for climate protection. For industrial applications, we have considered the integration of CO_2 absorption from AMP solutions into existing industrial production processes to minimize carbon emissions. The successful application of this technology will have a positive impact on the sustainable development of the industry and will drive further innovations in environmental protection technologies.

2. Numerical simulation

2.1. Physical model and boundary condition

After a comparative study with other common fillers, it has been determined that the Mellapak 250Y-type filler exhibits high surface area, low pressure drop, even distribution, pollution resistance, and corrosion resistance. These characteristics contribute to the outstanding performance of the Mellapak 250Y-type filler in gas-liquid mass transfer. Consequently, the Mellapak 250Y-type filler is employed, with the filler plate's dop angle set at 45°. The specific geometric parameters of the filler are provided in Table 1. To create a 3D model of the filler layer, the unit structure is simulated using ICEM CFD software, as depicted in Fig. 1-A.

Table 1. Mellapak250Y packing layer geometric parameters

Specific surface area / ($m^2 \cdot m^{-3}$)	Porosity /%	Bevel length /m	Tilt angle / (°)
250	97	0.0135	45

The unit model does not have a smooth wall surface; instead, it contains multiple bends. As a

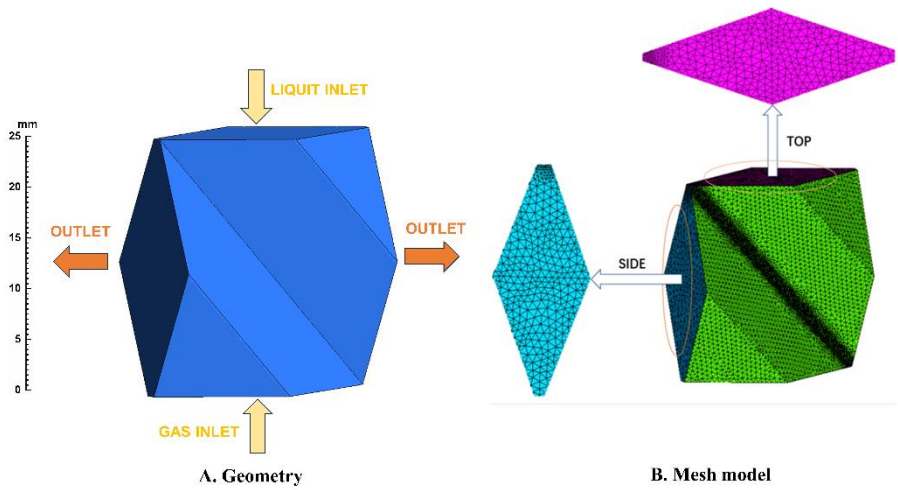

result, unstructured meshing is adopted, and the grid chart is displayed in Fig. 1-B.

Fig. 1. Model

In this research, the independence of the computational grid is taken into account. Fig. 2 shows

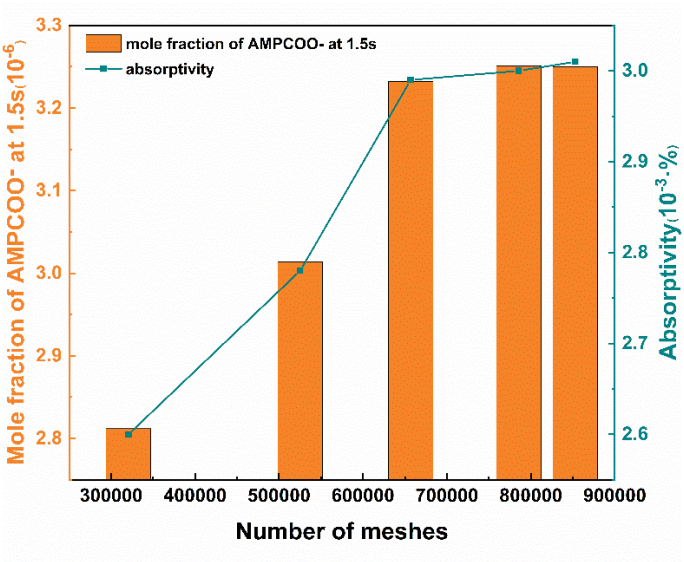

the CO_2 uptake rate for different numbers of grids.

Fig. 2. CO_2 absorption rate at different grid numbers

The trend chart in Fig. 2 reveals that as the number of grids increases, the CO_2 yield also rises. When the number of grids reaches 656,772, the CO_2 yield stabilizes. Therefore, the adoption of 656,772 units for the number of grids in this research has a minimal impact on the research results.

The boundary conditions are obtained from Huaneng carbon capture test research [22]. As depicted in Fig. 1-A, the top of the model serves as the liquid phase inlet, the bottom as the gas phase inlet, and both the left and right sides act as pressure outlets. The gas phase is designated as the dominant phase, while the liquid phase is considered the secondary phase. The basic pressure is set to 1 standard atmospheric pressure (101,325 Pa). Taking gravity into account, the gravitational acceleration is set at 9.8 m/s², acting in the negative y-axis direction. The specific boundary conditions are outlined in Table 2.

Table 2. Boundary conditions

The kind of boundary condition	Specific settings
Gas phase inlet	Using a speed inlet. The flue gas is set to CO_2 (16% mass fraction) and N_2 (84% mass fraction).

Liquid phase inlet	Using a speed inlet. The imported components are AMP (1% molar fraction) and water (90% molar fraction).
Chemical reaction	Using a component transport model and a general finite rate model, the operating temperature is 313 K, and the operating pressure is one standard atmospheric pressure (101325 Pa).

2.2. Fundamental equations and Turbulence model

Assuming that CO_2 behaves as an ideal gas, the AMP solution is an incompressible fluid, the transient reaction is established, and the ambient temperature remains constant throughout the entire reaction process, the mass conservation equation is as follows:

$$\frac{\partial(\alpha_k\rho_k)}{\partial t} + \nabla\cdot(\alpha_k\rho_k u_k) = S_k \#(\mathbf{1})$$

The momentum conservation equation is:

$$\frac{\partial(\alpha_k\rho_k u_k)}{\partial t} + \nabla\cdot(\alpha_k\rho_k u_k u_k) = -\alpha_k\nabla p + \nabla^2(\alpha_k u_k \mu_k) + \alpha_k\rho_k g_k + F_k \#(\mathbf{2})$$

The energy conservation equation is:

$$\frac{\partial(\alpha_k\rho_k h_k)}{\partial t} + \nabla\cdot(\alpha_k\rho_k u_k h_k) = \alpha_k\frac{\partial p}{\partial t} + \nabla\cdot(\lambda_k\nabla T_k) + Q_k + S_{e.k} \#(\mathbf{3})$$

In the FLUENT, the standard $k-\varepsilon$ model is selected:

$$\frac{\partial(\rho k)}{\partial t} + \frac{\partial k u_i}{\partial x_i} = \frac{\partial}{\partial x_j}\left[\left(\mu + \frac{\mu_t}{\sigma_k}\right)\frac{\partial k}{\partial x_j}\right] + G_k - \rho\varepsilon \#(4)$$

$$\frac{\partial(\rho\varepsilon)}{\partial t} + \frac{\partial(\rho\varepsilon u_i)}{\partial x_i} = \frac{\partial}{\partial x_j} + \left[\left(\mu + \frac{\mu_t}{\sigma_\varepsilon}\right)\frac{\partial\varepsilon}{\partial x_j}\right] + \frac{C_{1\varepsilon}\varepsilon}{k}G_K - C_{2\varepsilon}\rho\frac{\varepsilon^2}{K} \#(\mathbf{5})$$

2.3. Chemical reaction for CO_2 absorption by 2- amino-2-methyl -1 Propyl alcohol

The AMP solution is employed to capture CO_2 using two approaches: physical dissolution and chemical reaction. When the solution absorbs CO_2, several sequential reaction steps occur. The first thing that will be generated is the 2-amino-2-methyl-1-propyl alcohol carbamate ($AMPCOO^-$) and the combination of the protonated AMP($AMPH^+$) [23]:

$$CO_2 + 2AMP \rightarrow AMPCOO^- + AMPH^+ \#(6)$$

Due to its poor stability, the generated carbamic acid ester readily undergoes hydrolysis, yielding alcohol, amine, and bicarbonate ions:

$$AMPCOO^- + H_2O \rightarrow AMP + H_2CO_3 \#(7)$$

So, the total equation is:

$$CO_2 + AMP + H_2O \rightarrow AMPH^+ + H_2CO_3 \#(8)$$

The reaction equation indicates that the sterically hindered adhesive could theoretically absorb 1 mol of CO_2 per mole of sterically hindered amines after a specific CO_2 chemical dose. The process by which AMP absorbs CO_2 is relatively complex. Assuming that achieving this absorption is a secondary irreversible reaction during the simulation in FLUENT, the total equation can be simplified as follows:

$$CO_2 + 2AMP + H_2O \overset{k_2}{\rightarrow} AMPCOO^- + AMPH^+ \#(9)$$

The diffusion coefficient of carbon dioxide in AMP solution was calculated according to the method proposed by Saha [24] and Versteeg *et al.* [25] Simultaneously, the method proposed by Brent J. Sherman *et al.* [26] was used to determine the diffusion coefficient of AMP. Furthermore, through the experimental work of Kim *et al.* [27] ,it was possible to calculate the solubility of carbon dioxide.

2.4. Mass transfer model

In the contact process between AMP and CO_2, the gas phase and liquid phase come into contact with each other in a highly turbulent state. During this phase, there is no stable phase interface. Higbie [28] proposed the penetration theory, which treats interphase mass transfer as a dynamic process and describes the unsteady mass transfer process between the two phases. Consequently, the unsteady diffusion model is adopted in Fluent for simulation purposes.

The solute undergoes a 1D unsteady diffusion process within the fluid unit. When it diffuses to the gas-liquid interface, CO_2 is involved in a secondary chemical reaction. The rate of generation for CO_2 and AMP is:

$$r_{CO_2} = -k_2 c_{CO_2} c_{AMP} \#(10)$$

$$r_{AMP} = -2k_2 c_{CO_2} c_{AMP} \#(11)$$

The mass transfer differential equation of CO_2 could be expressed as

$$D_{CO_2}^{Solution} \frac{\partial^2 c_{CO_2}}{\partial y^2} = \frac{\partial c_{CO_2}}{\partial t} - r_{CO_2} \#(12)$$

This reaction can be categorized as an instantaneous reaction with a high reaction rate, allowing us to consider their diffusion coefficients as consistent. According to the solute permeability theory, the following mass transfer coefficient can be calculated:

$$k_{L,CO2} = \left(1 + \frac{c_{AMP}}{2c_{CO_2,\ i}}\right)\left(\frac{4D_{CO_2}}{\pi\theta_c}\right) \#(13)$$

The mass transfer coefficient is substituted into the mass source item, S_k

$$S_k = \frac{Mk_{L,CO2}AC_L\left(c_{CO_2,\ i} - c_{CO_2 0}\right)}{V} \#(14)$$

3. Simulation results of CO_2 absorption by 2- amino-2-methyl-1-propyl alcohol

3.1. Distribution condition of internal components of the unit model at different times

CO_2 is introduced into the model from the bottom, facilitating its interaction with the AMP solution flowing in from the top. During this reaction process, there is mass transfer between the gas and liquid phases, where the gaseous CO_2 is absorbed into the liquid phase and reacts. Based on the overall reaction equation, 1 mole of CO_2 generates 1 mole of $AMPCOO^-$ after the reaction. Consequently, the CO_2 absorption efficiency can be assessed on the basis of the production of

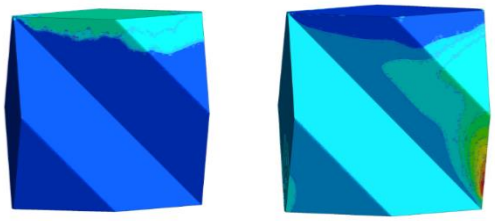

Fig. 3. At 0.5s，Distribution of AMP

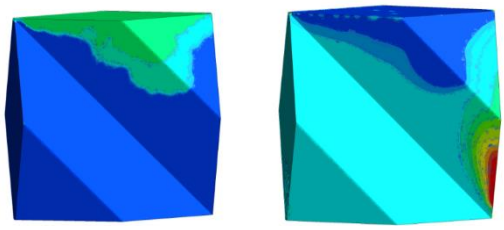

Fig. 4. At 1.0s，Distribution of AMP (left) and CO_2 (right)

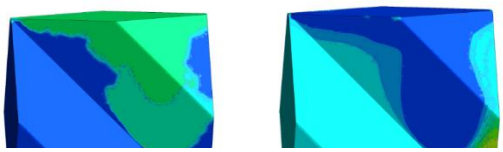

Fig. 5. At 1.5s，Distribution of AMP

$AMPCOO^-$. The conversion rate of carbon dioxide is approximately equal to the molar fraction of ammonium bicarbonate on the filler's surface at steady state, divided by the molar fraction of carbon dioxide.

At a gas flow velocity of 0.5526 m/s, the internal distribution of AMP and CO2 within the model at 0.5s, 1.0s, and 1.5s can be observed, as depicted in Figs. 3 to 5.

At 0.5 s, AMP is concentrated at the top of the model, while CO_2 occupies most of the model. With the ongoing reaction and under the influence of gravity, the AMP solution starts flowing downward, as illustrated in Figs. 4 and 5, resulting in a gradual reduction of the area occupied by CO_2.

3.2. Influence of molar fractions of different AMPs on the CO_2 absorptivity

To investigate the relationship between the molar fraction of AMP and the absorption efficiency of a unit model, the molar fraction of AMP was adjusted without altering other boundary conditions. The flue gas rich in CO_2 had a flow velocity of 0.5526 m/s, the liquid had a flow velocity of 0.00737 m/s, and the mass fraction of CO_2 in the flue gas was 16%. The pressure was set at standard atmospheric pressure, and the temperature was set at 313K. AMP molar fractions were set to 0.04, 0.1,

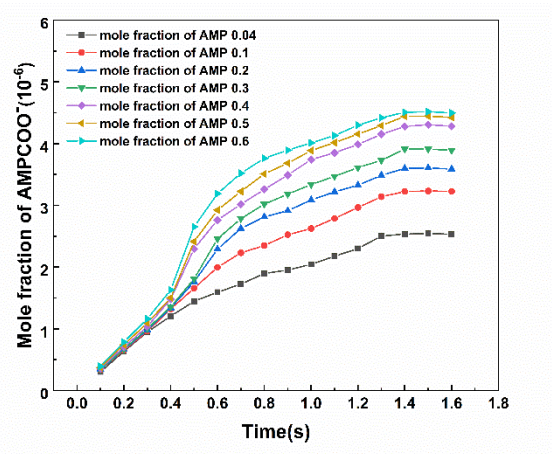

Fig. 6. Production of AMPCOO$^-$ within 0 ~ 1.6s at different AMP

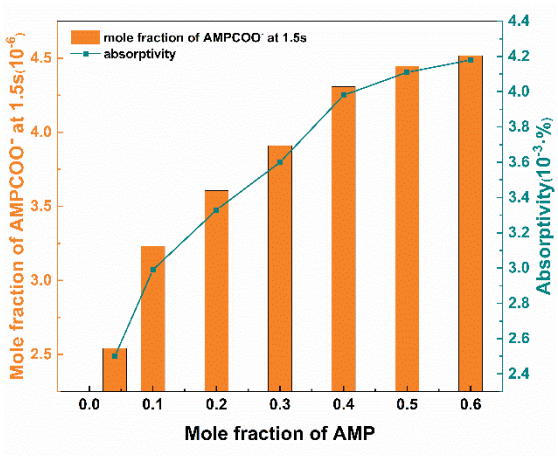

Fig. 7. CO_2 absorption rate calculated at different AMP concentrations

0.2, 0.3, 0.4, 0.5, and 0.6, respectively.

Figure 6 reveals that, within 1.6 seconds, the AMPCOO$^-$ content continuously rises. Before 0.4 seconds, there is a slight increase in yield due to the necessary time for the liquid and gas phases to come into contact. After 0.4 seconds, the two-phase fluid begins to make full contact, and the reaction accelerates. However, when the AMP molar fraction is between 0.4 and 0.6, the increase in AMPCOO$^-$ yield gradually slows down.

Figure 7 indicates that CO_2 absorptivity increases rapidly when the AMP molar fraction is between 0.04 and 0.4, but the absorptivity of CO_2 uptake gradually slows down at AMP molar fractions of 0.4 to 0.6. From a chemical reaction equilibrium perspective, an increase in AMP molar concentration leads to an increase in the molar ratio of AMP to CO_2, promoting the chemical reaction towards the right and enhancing CO_2 absorptivity. From a macro perspective, the two-phase fluid reacts rapidly upon initial contact, which leads to higher mass transfer rates at the gas-liquid interface and within the liquid phase, ultimately leading to an increase in CO_2 absorptivity.

3.3. Influence of different ambient pressures on CO_2 absorptivity

To investigate the influence of ambient pressure on the absorption efficiency of a unit model, the ambient pressure is systematically adjusted by keeping all other boundary conditions constant. The

ambient pressure was varied to values of 0.2, 0.5, 1, 1.5, and 2.0 atmospheres to thoroughly explore their impact on absorption efficiency.

Analyzing Fig. 8, it is evident that the entire reaction process accelerates starting at 0.3 seconds

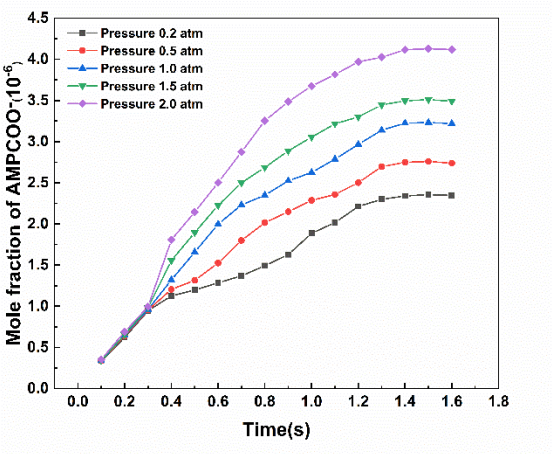

Fig. 8. Production of AMPCOO$^-$ within 0 ~ 1.6s

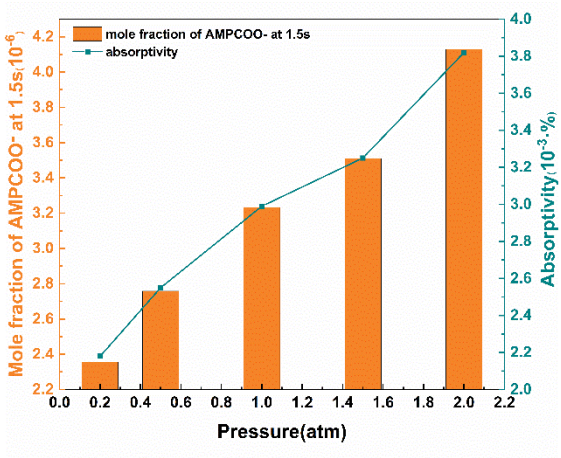

Fig. 9. CO_2 absorption rate calculated at different ambient pressures

and reaches a state of stability between 1.3 and 1.6 seconds. Correlating this with Fig. 9, an increase in ambient pressure corresponds to a higher AMPCOO$^-$ yield at 1.5 seconds and increased CO_2 absorptivity. This can be attributed to several factors from a chemical reaction perspective: Increased pressure shifts the chemical equilibrium towards the right, intensifying the reaction rate, allowing for more effective interactions between the absorbent and gas. On a molecular level, higher pressure equates to more gas molecules within the same volume, resulting in more frequent and effective collisions between gas and liquid, consequently speeding up the reaction rate and increasing product quantities.

3.4. Influence of different gas velocities on CO2 absorptivity

To conduct an in-depth investigation into the interrelation between air velocity and CO_2 absorptivity within a unit model, the gas flow velocity is systematically regulated while maintaining all other boundary conditions constant. Gas flow velocities are set at 0.0737, 0.5526, 0.8844, 1.1055, 1.2529, and 1.474 m/s, corresponding to 10, 75, 120, 150, 170, and 200 times the liquid flow velocity.

Figure 10 reveals that the AMPCOO$^-$ relatively stable trend of production increased within the 0 to 1.6-second interval. When considering Fig. 11 in conjunction, it becomes apparent that as gas flow velocity increases, the output of AMPCOO$^-$ diminishes, resulting in a continuous decrease in CO_2 absorptivity.

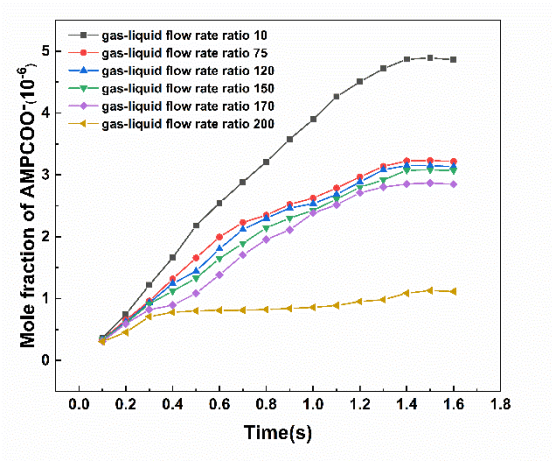

Fig. 10. Production of AMPCOO$^-$ within 0 ~ 1.6s at different gas flow rates

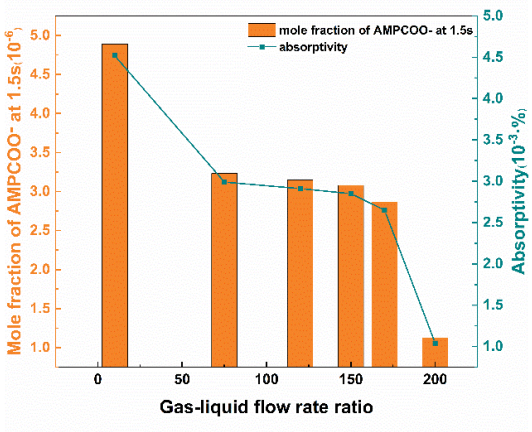

Fig. 11. CO_2 absorption rate calculated at different gas flow rates

Augmenting the gas flow velocity facilitates a more rapid interaction between the gas and liquid phases; however, it also reduces the reaction time between the gas and liquid in the unit model. This increased velocity may result in some absorbents being blown out of the model by the high-speed gas. Consequently, relatively lower gas velocities are favored in industrial production to enhance CO_2 absorptivity. In the unit simulation, the reaction site is defined as the inner surface of the model. The higher gas flow velocities cause the liquid to remain primarily on the upper surface of the model, preventing it from fully covering the surface of the model, resulting in insufficient CO_2 uptake.

3.5. Influence of different CO2 mass fractions on CO2 absorptivity

After conducting research on the influence of different AMP concentrations, ambient pressures, and gas flowing velocities on the CO_2 absorptivity of a unit model, it is essential to further investigate the relationship between the CO_2 mass fraction and the model. The CO_2 mass fraction was set to 0.12, 0.14, 0.15, 0.16, and 0.19, respectively.

Figure 12 reveals that the content of the product AMPCOO$^-$ remains nearly constant between 0 and 0.3 seconds for different CO_2 mass fractions. However, the difference in AMPCOO$^-$ content within the range of 0.3 to 1.5 seconds increases gradually with varying CO_2 mass fractions. Combining this with Fig. 13, it can therefore be concluded that the absorptivity of CO_2 decreases as the CO_2 mass fraction increases.

During the reaction process, an increase in the mass fraction of CO_2 signifies a higher initial concentration of CO_2, which in turn enhances the molar ratio of CO_2 and AMP. From the perspective of chemical reaction equilibrium, this results in a decrease in the overall reaction rate, which is unfavorable for CO_2 absorption and leads to a reduction in CO_2 absorptivity.

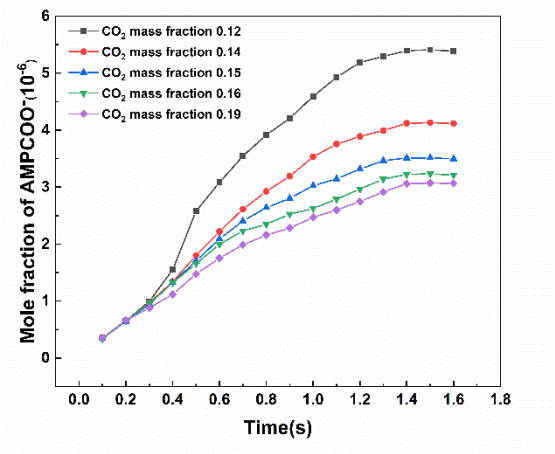

Fig. 12. Production of AMPCOO$^-$ within 0 ~ 1.6s at different CO_2 mass fractions

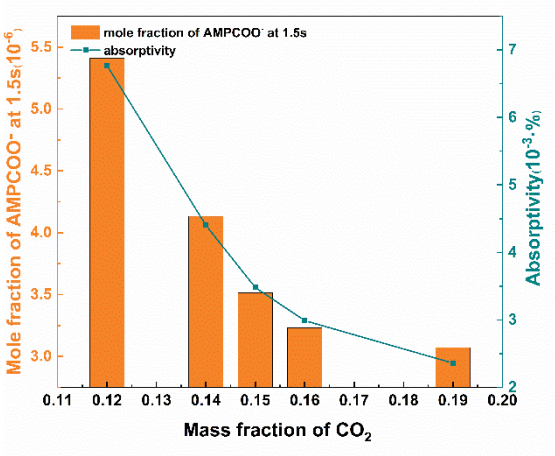

Fig. 13. CO_2 absorption rate calculated at different CO_2 mass fractions

Additionally, an increase in CO_2 mass fraction means an elevation in the concentration of CO_2 at the unit model's gas inlet and the CO_2 partial pressure. Consequently, more CO_2 enters the AMP solution for reaction. However, this increase in the gross amount of CO_2 entering the AMP solution cannot offset the impact of the higher initial concentration of CO_2. As a result, the overall CO_2 absorptivity decreases as the CO_2 mass fraction rises.

3.6. Analysis of optimal parameters

The absorption of CO_2 in flue gas is analyzed under four different conditions in the above simulation. To investigate the absorption behavior of CO_2 in flue gas under the combined influence of these different conditions, the AMP mole fraction, ambient pressure, gas flow rate, and CO2 mass fraction are denoted by A, B, C, and D, respectively. High and low values were selected for each condition, resulting in 16 (2^4=16) distinct simulation scenarios through permutation and combination. The specific simulation scenarios and the corresponding CO_2 absorptivity are presented in Table 3.

Table 3. Simulation results

Number	A	B/KPa	C/m·s^{-1}	D/wt%	Absorptivity/%
1	0.04	20.265	0.0737	0.12	0.00382
2	0.04	20.265	0.0737	0.19	0.00292
3	0.04	20.265	1.474	0.12	0.00308
4	0.04	20.265	1.474	0.19	0.00211
5	0.04	202.65	0.0737	0.12	0.00426

6	0.04	202.65	0.0737	0.19	0.00374
7	0.04	202.65	1.474	0.12	0.00361
8	0.04	202.65	1.474	0.19	0.00297
9	0.6	20.265	0.0737	0.12	0.00628
10	0.6	20.265	0.0737	0.19	0.00386
11	0.6	20.265	1.474	0.12	0.00602
12	0.6	20.265	1.474	0.19	0.00377
13	0.6	202.65	0.0737	0.12	0.00724
14	0.6	202.65	0.0737	0.19	0.00437
15	0.6	202.65	1.474	0.12	0.00616
16	0.6	202.65	1.474	0.19	0.00415

Table 2 clearly illustrates that the highest values are chosen for conditions A and B, leading to the maximum absorptivity obtained through simulation when lower values were chosen for conditions C and D. When combining these findings with the analysis of absorptivity under individual conditions, it was found that the absorptivity increased insignificantly within the AMP molar fraction range of 0.4 to 0.6. Furthermore, the absorptivity continues to rise as the pressure increases.

However, considering that a pressurizing device is needed to increase the pressure inside the container. Therefore, it should be recommended that the AMP molar fraction be at 0.4, the pressure be at normal atmospheric levels, setting the flue gas flow velocity be set at 0.0737 m/s, and the CO_2 mass fraction be set at 0.12.

4. Conclusion

In this paper, a unit model was constructed inside the absorption tower with a grid system, and the appropriate number of grids was determined by grid independence validation. The grid model has been imported into FLUENT for simulation, and the product distribution cloud map at different gas phase velocities can be observed.

The boundary conditions were modified to simulate the CO_2 absorption conditions of the AMP solution within the unit model under different scenarios. The influencing factors were analyzed to determine CO_2 absorptivity under 16 different simulation conditions. The results indicate that absorptivity increases with higher AMP molar fractions and ambient pressure, while it decreases with

higher gas phase velocities and CO_2 mass fractions. Considering the relatively challenging operation of increased pressurizing equipment, the following rational and optimal parameters were comprehensively considered: an AMP molar fraction of 0.4, ordinary pressure for the set pressure, a flue gas flow velocity of 0.0737 m/s, and a CO_2 mass fraction of 0.12. Even though we set some parameters in our numerical simulations, we have to be honest and admit that this limitation may have some impact on our study. However, we cannot ignore the potential uncertainties that the inability to set parameters may introduce. In future studies, we plan to work on this issue and explore ways to integrate the actual operating parameters more accurately.

Nomenclature

A-cell contact area, [m^2]

C_L- total molar concentration of solution, [mol/m^3]

$c_{CO_2,\ i}$- the concentration of CO_2 on interface, [mol/m^3]

$c_{CO_2 0}$ - the concentration of CO_2 on liquid body, [mol/m^3]

F_k-interphase interaction force, [N]

G_k-turbulence energy resulting from mean velocity gradient, [m^2/s^2]

h_k-specific enthalpy of the kth substance, [J/mol]

g_k-gravity volume force, [m/s^2]

$D_{CO_2}^{Solution}$- diffusion coefficient of CO_2 in solution, [m^2/s]

$k_{L,CO2}$-mass transfer coefficient of CO_2

k-turbulent kinetic energy, [m^2/s^2]

M-the molar mass of CO_2, [kg/mol]

p-static pressure, [Pa]

Q_k-interphase heat conduction intensity, [J/kg]

r_{CO_2}- The rate of generation for CO_2, [mol/(L·s)]

r_{AMP}- The rate of generation for AMP, [mol/(L·s)]

S_k- mass source term, [$kg/m^3 \cdot s$]

$S_{e,k}$-enthalpy source term in chemical reactions, [$J/m^3 \cdot s$]

S_m-quality source items, [$kg/ m^3 \cdot s$]

u_k-velocity vector,[m/s]

V- the cell volume, [m^3]

ρ_k-the density of the kth phase, [kg/m^3]

μ_k-dynamic viscosity, [$N \cdot s/m^3$]

λ_k-thermal conductivity, [W/m·K]

θ_c-length of stay, [t]

ε-dissipation rate, [m/s]

σ_k-turbulent kinetic energy k turbulent Planter number, [-]

σ_ε-turbulent Planter number of dissipation rate ε, [-]

References

[1] Zou, C., *et al.*, Energy revolution: From a fossil energy era to a new energy era, *Natural Gas Industry B*, 3 (2016), 1, pp. 1-11

[2] Bragatto, T., *et al.*, Electrical Energy Production from Coal: Technical and Economic Performances during the Last Twenty Years, "2022 IEEE International Conference on Environment and Electrical Engineering and 2022 IEEE Industrial and Commercial Power Systems Europe (EEEIC / I&CPS Europe), Prague, Czech Republic, 2022, pp. 1-6

[3] Andrew, R. M., Global CO2 emissions from cement production, 1928–2018, *Earth System Science Data*, 11 (2019), 4, pp. 1675-1710

[4] Mersin, K., *at al.*, Review of CO2 emission and reducing methods in maritime transportation, *Thermal Science*, 23 (2019), 6, pp. S2073-S2079

[5] Wang, Y., et al., Integrated assessment of CO2 reduction technologies in China's cement industry, *International Journal of Greenhouse Gas Control*, 20 (2014), pp. 27-36

[6] Guo, J., *et al.*, Numerical investigation on oxy-combustion characteristics of a 200MWe tangentially fired boiler, *Fuel*, 140 (2015), pp. 660-668

[7] Wang, T., *et al.*, Amine reclaiming technologies in post-combustion carbon dioxide capture, *Journal of Environmental Sciences*, 27 (2015), pp. 276-289

[8] Cui, Z., *et al.*, Waste heat recovery and cascade utilization of CO2 chemical absorption system based on organic amine method in heating season, *Applied Thermal Engineering*, 230 (2023), p. 120834

[9] Zhou, X., *et al.*, Multi-dimensional assessment for the novel carbon capture process integrated the low-temperature adsorption and desorption, *Chemical Engineering Science*, 282 (2023), p. 119207

[10] Luis, P., Use of monoethanolamine (MEA) for CO 2 capture in a global scenario: Consequences and alternatives, *Desalination*, 380 (2016), pp. 93-99

[11] Benamor, A., Aroua, M. K., An experimental investigation on the rate of CO2 absorption into aqueous methyldiethanolamine solutions, *Korean Journal of Chemical Engineering*, 24 (2007), 1, pp. 16-23

[12] Feng, Z., *et al.*, Absorption of CO2 in the aqueous solutions of functionalized ionic liquids and MDEA, *Chemical Engineering Journal*, 160 (2010), 2, pp. 691-697

[13] Kierzkowska-Pawlak, H., Chacuk, A., Kinetics of CO2 desorption from aqueous N-methyldiethanolamine solutions, *Chemical Engineering Journal*, 168 (2011), 1, pp. 367-375

[14] Ahmady, A., *et al.*, Kinetics of Carbon Dioxide absorption into aqueous MDEA+[bmim][BF4] solutions from 303 to 333K, *Chemical Engineering Journal*, 200-202 (2012), pp. 317-328

[15] Glazyrin, S. A., *et al.*, Study of the possibilities of integrated treatment of flue gases and waste water from coal-fired heat power plants, *Thermal Science*, 25 (2021), 6A, pp. 4333-4345

[16] Bougie, F., Iliuta, M. C., Sterically Hindered Amine-Based Absorbents for the Removal of CO2 from Gas Streams, *Journal of Chemical & Engineering Data*, 57 (2012), 3, pp. 635-669

[17] Conway, W., *et al*., Toward the Understanding of Chemical Absorption Processes for Post-Combustion Capture of Carbon Dioxide: Electronic and Steric Considerations from the Kinetics of Reactions of CO2 (aq) with Sterically hindered Amines, *Environmental Science & Technology*, 47 (2013), 2, pp. 1163-1169

[18] Bougie, F., Iliuta, M. C., Kinetics of absorption of carbon dioxide into aqueous solutions of 2-amino-2-hydroxymethyl-1,3-propanediol, *Chemical Engineering Science*, 64 (2009), 1, pp. 153-162

[19] Sartori, G., Savage, D. W., Sterically hindered amines for carbon dioxide removal from gases, *Industrial & Engineering Chemistry Fundamentals*, 22 (1983), 2, pp. 239-249

[20] Khan, A. A., *et al.*, Carbon dioxide capture characteristics from flue gas using aqueous 2-amino-2-methyl-1-propanol (AMP) and monoethanolamine (MEA) solutions in packed bed absorption and regeneration columns, *International Journal of Greenhouse Gas Control*, 32 (2015), pp. 15-23

[21] Jamali, M., Azari, A., A Review on Computational Fluid Dynamics Simulations of Industrial Amine Absorber Columns for CO2 Capture, *Chembioeng Reviews*, 10 (2023), 1, pp. 6-21

[22] Huang, B., *et al.*, Industrial test of CO2 capture in Huaneng Beijing coal-fired power station, *Proceedings of the CSEE*, 29 (2009), 17, pp. 14-20

[23] Vaidya, P. D., Jadhav, S. G., Absorption of carbon dioxide into sterically hindered amines: Kinetics analysis and the influence of promoters, *The Canadian Journal of Chemical Engineering*, 92 (2014), 12, pp. 2218-2227

[24] Saha, A. K., *et al.*, Solubility and diffusivity of nitrous oxide and carbon dioxide in aqueous solutions of 2-amino-2-methyl-1-propanol, *Journal of Chemical and Engineering Data*, 38 (1993), 1, pp. 78-82

[25] Versteeg, G. F., Van Swaaij, W. P., Solubility and diffusivity of acid gases (carbon dioxide, nitrous oxide) in aqueous alkanolamine solutions, *Journal of Chemical & Engineering Data*, 33 (1988), 1, pp. 29-34

[26] Sherman, B. J., Rochelle, G. T., Thermodynamic and Mass-Transfer Modeling of Carbon Dioxide Absorption into Aqueous 2-Amino-2-Methyl-1-Propanol, *Industrial & Engineering Chemistry Research*, 56 (2017), 1, pp. 319-330

[27] Kim, Y. E., *et al.*, Comparison of Carbon Dioxide Absorption in Aqueous MEA, DEA, TEA, and AMP Solutions, *Bulletin of the Korean Chemical Society*, 34 (2013), 3, pp. 783-787

[28] Higbie, R., The Rate of Absorption of a Pure Gas into a Still Liquid during Short Periods of Exposure, *Trans. AIChE*, 31 (1935), pp. 365-389

Submitted: 09.11.2023.
Revised: 07.01.2024.
Accepted: 15.01.2024.